Investigating the Noise Sources of the Transonic RAE 2822 Airfoil

Antonio Alguacil[1+], Lorenzo Becherucci[1], Marlène Sanjosé[2], Stéphane Moreau[1*]

[1]Mechanical Engineering Department, Université de Sherbrooke, Sherbrooke, QC, J1K2R1, Canada
[2]Mechanical Engineering Department, École de Technologie Supérieure, Montréal, QC, H3C1K3, Canada
[+]antonio.alguacil.cabrerizo@usherbrooke.ca
[*]stephane.smoreau@gmail.com

Abstract—A compressible Large Eddy Simulation is performed on the transonic RAE 2822 airfoil, and compared to the baseline simulation of Koch *et al.* (28th AIAA/CEAS Aeroacoustics Conference, paper AIAA 2022–2816) in order to highlight the main noise source mechanisms. The new simulation employs a new mesh which eliminates a jump in the airfoil surface mesh, located in the supersonic laminar boundary layer region of the suction side. This jump induced some hydrodynamic instability in the suction side boundary layer of the baseline simulation, potentially emitting noise at high-frequencies. The new results show that these instabilities are significantly damped when employing the new refined mesh and are consequently very sensitive to the grid quality. Nonetheless, the acoustic response of the airfoil, calculated using the Ffowcs Williams and Hawkings analogy in its solid formulation, remains similar to the baseline, with a high-frequency hump appearing between 30 and 40 kHz. This shows that this hump is not caused by the hydrodynamic instabilities, therefore confirming the grid independence of the acoustic results.

Keywords-component—Transonic flows; RAE 2822 airfoil; aeroacoustics; Large-Eddy Simulations

I. INTRODUCTION

Transonic airfoils are employed in aeronautical applications where the flow reaches supersonic conditions locally, typically for free-flow Mach numbers between 0.7 and 0.9. They can be found in commercial aircraft wings, helicopter blades [1] or at the tip of turbofans blades tip [2], where the flow may reach supersonic conditions during take-off. The design of such airfoils aims at improving the aerodynamic efficiency by reducing the shock-boundary layer interaction appearing at its suction side.

A typical transonic airfoil geometry is the RAE 2822 supercritical airfoil, developed by the National Air and Space Administration (NASA). Several experimental and numerical works investigated the aerodynamic features of this airfoil. Cook *et al.* [3] conducted an experimental campaign, obtaining the pressure distribution for various angles of attack and in-flow Mach numbers. Later, steady Reynolds-Averaged Navier-Stokes (RANS) simulations were performed by Catalano and Amato [4], where the ability of several turbulence models to correctly reproduce the flow around such an airfoil was assessed. Yu *et al.* [5] also performed RANS simulations on the flow around the RAE 2822 airfoil, investigating the effects of a Gurney flap on its aerodynamic performance.

Unsteady numerical methods have also been applied to this airfoil. Xiao *et al.* [6] performed a Detached Eddy Simulation to investigate the ability of the weakly nonlinear eddy-viscosity formulated k-ω WD+ model to predict the transonic shock-wave and boundary-layer interaction flows. Furthermore, Tonicello [7] achieved a wall-resolved unsteady simulation with Large-Eddy Simulation (LES) on the RAE 2822 to test a new efficient shock-capturing algorithm for high-order turbulent simulations. In the latter, the main flow mechanisms occurring close to the shock/boundary layer interaction were highlighted. There, wave roll-ups structures start to develop, which finally break up in fully turbulent vortices downstream of the shock.

Recently, Koch *et al.* [8] performed the first numerical acoustic investigation on the noise sources of this transonic airfoil with a compressible wall-modeled LES simulation. A very good agreement was found on the mean pressure coefficient with previous experimental and numerical results. Furthermore, four possible acoustic sources were identified in a preliminary study. First, the airfoil self-noise, due to the scattering of the turbulent boundary layer eddies at the trailing edge, was established as the main source of noise in the mid-to-high frequency range ($10^3 - 10^4$ Hz). The sound source arising from the interaction of the shock wave and the

boundary layer at the airfoil suction side is identified as the second candidate. However, it was found that its quadrupolar contribution is negligible versus the self-noise at the vertical of the airfoil. Third, a possible high-frequency source arising from the boundary layer transition on the pressure side was observed with two peaks at 20−30 kHz and 50 kHz in the wall-pressure Power Spectral Density (PSD). Nonetheless, such near field measurements were not correlated to far-field noise measurements, thus the radiation from such a source could not be confirmed. Finally, a fourth possible noise source candidate was identified with a high-frequency peak (30 − 40 kHz) present in the far-field pressure PSD, for two probes located upstream of the airfoil. The origin of such peak in the far-field noise spectrum remains unclear, since it cannot be attributed to the dominant trailing edge dipolar source. Therefore, some uncertainties remain around the complete characterization of the acoustic sources in the RAE 2822 airfoil.

The objective of this work is to extend the previous analysis [8] in order to remove some of the uncertainties related to candidate acoustic sources. In particular, the focus is put on validating the presence of the high-frequency sources, which are visible in the far-field spectra upstream of the airfoil. The paper is organized as follows: Section II presents the numerical setup, comparing the baseline mesh of Koch *et al.* [8] with a new mesh where a refinement is performed in the suction side region of the airfoil. Section III presents the aerodynamic results, both steady and unsteady, comparing the new LES performed on the refined mesh with the baseline simulation. Finally, Section IV discusses the acoustic results.

II.   NUMERICAL SETUP

The numerical configuration is composed of a RAE 2822 airfoil of 50 mm span and 304.8 mm chord placed in a 3 m × 5 m numerical domain. The coordinate system is labeled (0, X, Y, Z) and is centered on the airfoil leading edge. The X axis follows the streamwise inflow direction (pointing from the leading edge to the trailing edge), the Y axis is normal to the X axis (pointing from the pressure side to the suction side), and the Z axis follows the spanwise direction. A midspan view of the numerical domain is shown in Fig. 1.

The previous work [8] performed two simulations, a steady RANS (using the ANSYS CFX solver) and a LES, using the AVBP solver [9]. A reminder of the numerical parameters employed in the LES simulation, dubbed LES 1, is given next.

II-A   LES 1: Baseline

LES 1 employed a hybrid mesh, using 66.8×10^6 cells with 13 prismatic layers, with a maximum expansion ratio of 1.15. Since the LES used a wall model, the wall resolution was set to $y^+ < 30$, which is maximum at the shock position and around 15 on the rest of the airfoil. The average surface mesh size reached 0.4 mm in order to have a maximum aspect ratio of 10 for the first cell at the wall. Refinement zones were located around the airfoil, in the wake, and in the shock region, with a mesh size from 0.25 to 0.5 mm in the vicinity of the shock. The mesh is depicted in Fig. 2a.
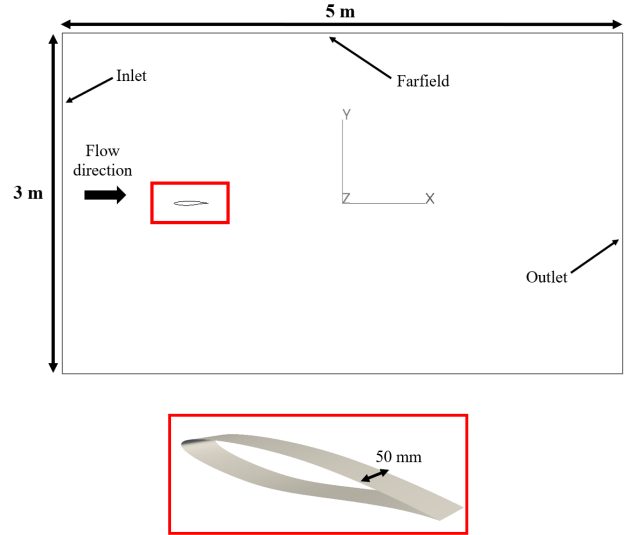

Figure. 1: Numerical domain used for the simulations.

Furthermore, the numerical scheme employed was the explicit Lax-Wendroff (LW) scheme, which is second order in space and in time. The time step was fixed at 1.6×10^{-8} s which guaranteed a maximum CFL of 0.9 in the whole domain for stability reasons. Non-reflective Navier-Stokes characteristic boundary conditions (NSCBC) [10] were used at the inlet and the outlet, combined with a sponge layer at the end of the domain to avoid spurious reflections [11]. At the subsonic inlet, static pressure P_∞ = 108,987 Pa, static temperature T_∞ = 255.6 K, and velocity components were imposed. The inflow Reynolds number based on chord is 6.5×10^6, the inflow Mach number is 0.725, and the angle of attack is 2.91°. These parameters correspond to the test case number 6 in [3]. In the far-field and at the outlet, static pressure P_∞ was imposed. Translation periodicity was imposed on both sides of the domain to reproduce an infinite span airfoil and reduce the computational cost. In order to have the proper turbulence decay toward the walls, the sub-grid scale model used was the Wall-Adapting Local Eddy-viscosity model (WALE) [12].

II-B   LES 2: Refined mesh

A new LES, dubbed LES 2, is performed in this work in order to validate or discard the high-frequency noise sources found in [8]. This new simulation is justified by the following observation: the LES 1 surface mesh was refined around the leading edge (for X/c < 0.1), as shown in Fig. 2b (top mesh). However, a sharp transition in the surface mesh can be observed between the refined region and the coarser one at mid-chord. This transition may induce non-physical flow features in the suction side of the airfoil, and may also trigger some spurious acoustic sources. In order to investigate this issue, a new mesh is employed in the LES 2 simulation. It eliminates the sharp transition by extending the refinement region around the leading edge until X/c < 0.4, with a gradual coarsening of the surface grid size. The resulting surface mesh can be seen in Fig. 2b (bottom mesh), while the final volumetric mesh employs 67.5×10^6 cells.
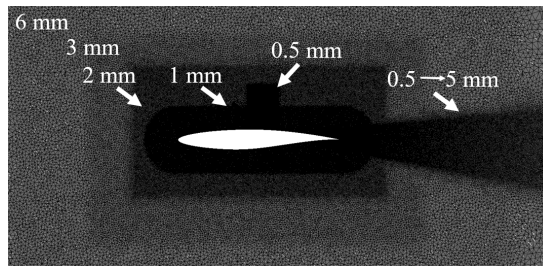
(a)
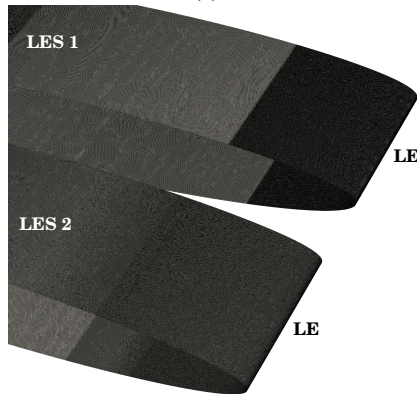
(b)

Figure. 2: Mesh- (a): (X,Y) cut of the LES 1 volumetric mesh at midspan (b): comparison of airfoil surface meshes for LES 1 and LES 2, seen from the suction side and centered around the leading edge.

The rest of the simulation parameters remain identical to LES 1, except for the time-step which is lowered to 8.4×10^{-9} in order to ensure a CFL number equal to 0.9 in the new mesh. Note also that the same Lax-Wendroff (LW) scheme (second order accuracy in space and in time) is employed. Thus, the main objective of this new simulation is to focus on the effects of the grid in the flow features and the acoustic sources.

III. AERODYNAMIC RESULTS

The baseline LES 1 simulation was run for 5 flow-through times based on the chord (about 7 ms) in order to establish the flow. After that, statistics for wall-pressure and far-field pressure spectra as well as mean and unsteady velocity fields were extracted during approximately 51 ms or 42 flow-through times based on the chord. For the LES 2 simulation, the solution at 35 ms of LES 1 is interpolated into the new LES 2 mesh. Th mid-range flow is established after 3 flow-through times based on the chord, and unsteady statistics are collected for the following 20 ms (16 flow-through times).

Figure 3 compares the aerodynamic results of LES 1 and LES 2, showing the Q-criterion (the second invariant of the gradient velocity tensor), viewing the suction side from the top of the airfoil. The results are colored with the Mach number. On the one hand, the results show that the boundary layer transition to turbulence happens at the same location in both cases, i.e. after the location of the shock-wave which causes a strong adverse pressure gradient. This turbulent boundary
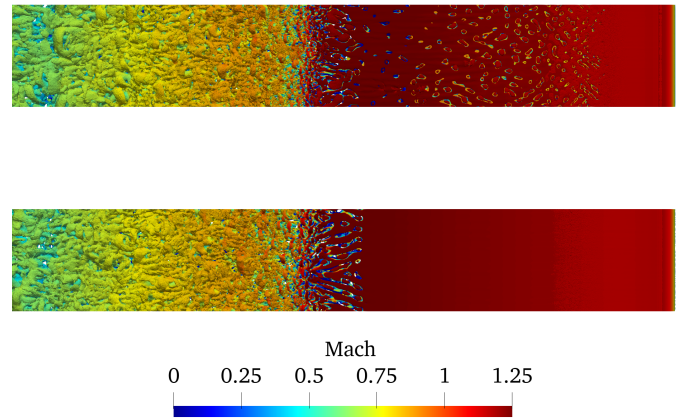

Figure. 3: Isosurface of instantaneous Q-criterion from LES 1 (top) and LES 2 (bottom) colored with the Mach number magnitude. View of the airfoil suction side. The air flows from right to left.
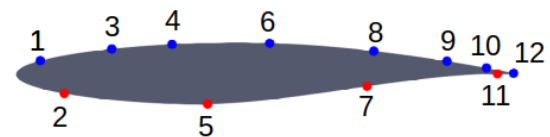

Figure. 4: Position of the probes

layer is convected passed the trailing edge, which was shown in [8] to be the main noise source mechanism at frequencies in the range of 1 to 10 kHz. On the other hand, the results differ on the laminar region of the airfoil (before the shock location). Indeed, while large-size oblique flow structures are observed in the LES 1 results, the visualization of the LES 2 does not show any trace of such coherent structures. These structures may be the trace of a flow instability appearing at the suction side, before the boundary layer transition. The difference in behavior between LES 1 and LES 2 suggests
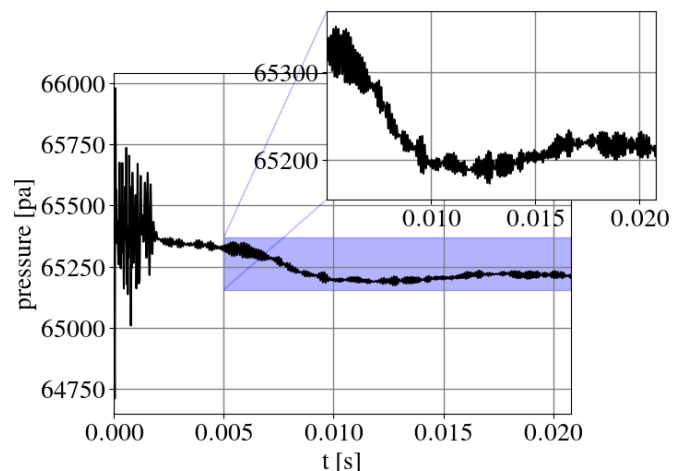

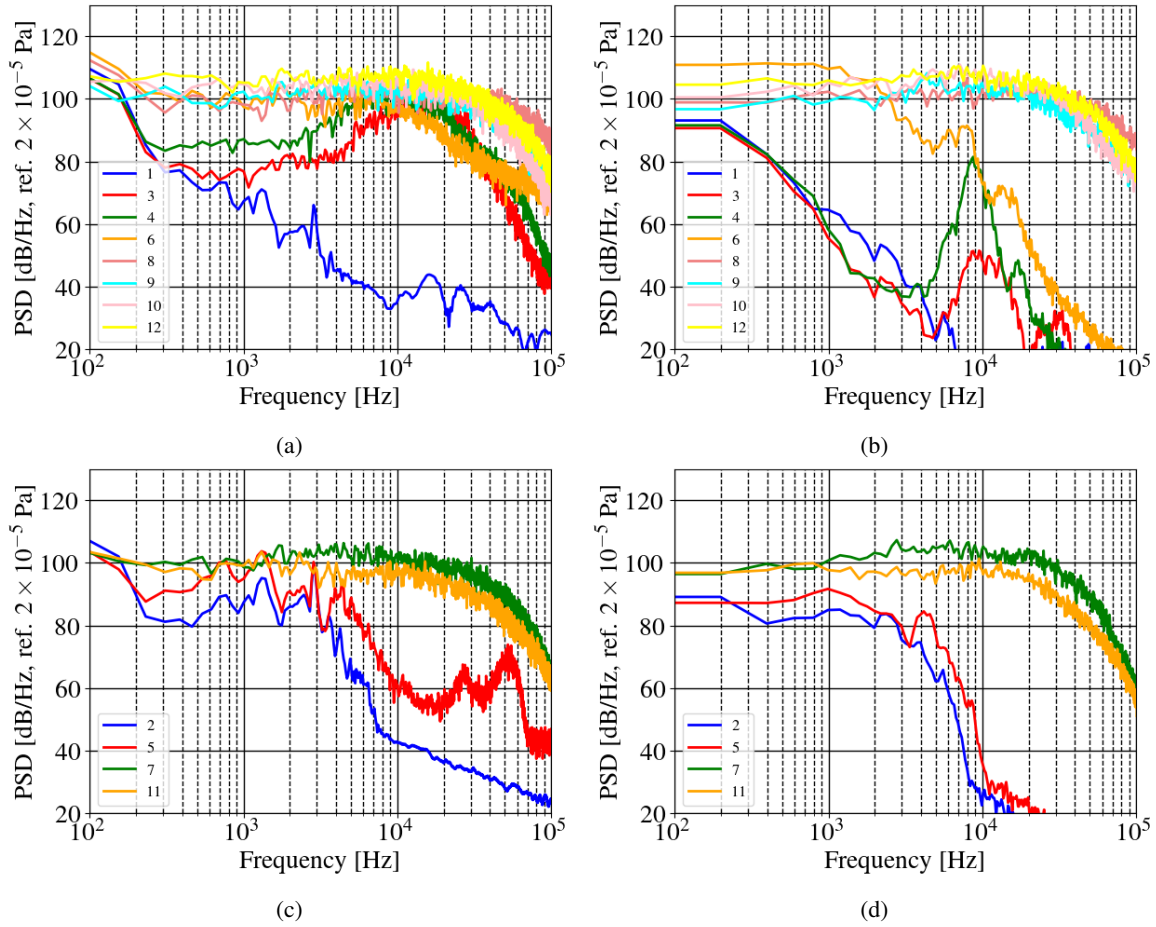Figure. 5: Temporal pressure signal at probe 4 (suction side).

Figure. 6: Wall-pressure PSD on the airfoil surface at midspan, for (a): LES 1 suction side; (b): LES 2 suction side; (c): LES 1 pressure side and (d): LES 2 pressure side.

that these instabilities are strongly enhanced by the jump in surface mesh, as shown in Fig. 2b. However, this claim must be further validated with more quantitative results, *i.e.* with wall-pressure measurements, which are shown next.
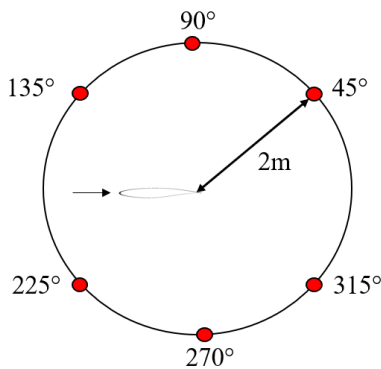

Figure. 7: Far-field probe location, centered around the airfoil trailing edge.

For that, probes are located on the suction and pressure sides of the airfoil as shown in Fig. 4, denoted by numbers 1–12. 8 of them are located in the the suction side and 4 in the pressure side. Note that the shock-wave is located between

probes 6 and 8 on the suction side. The wall-pressure signals for LES 1 are $T = 51$ ms long and are sampled at 625 kHz, while for LES 2, the signals are $T = 20$ ms long, sampled at 1,200 kHz. An example of time signal is shown in Fig. 5 for probe 4, located inside the supersonic pocket of the suction side. Note that small-amplitude oscillations are still visible after the initial transient. These oscillations confirm that some instability may persist in this airfoil region. Then, the wall-pressure PSD are compared between pressure and suction sides at different chord locations in Fig. 6, for LES 1 and LES 2. The PSD is obtained with Welch's periodogram method [13]. Time windows of length T/4 with 50% overlap are used to compute the PSD. It yields a total of 7 blocks, windowed with a Hanning function. The frequency resolution of the PSD spectra is thus equal to $\Delta f = 78$ Hz for LES 1 and $\Delta f = 200$ Hz for LES 2. For the suction side, probes after the shock-wave (8, 9, 10 and 12) show an identical behavior for both LES 1 and LES 2, confirming the previous observations about the transition of the boundary layer. However, in the probes located before the shock-wave (1, 3, 4 and 6), large differences are observed: a large hump could be observed centered around 10-15 kHz in probes 3 and 4 of LES 1. For LES 2, a sharper peak can be observed instead at 10 kHz, but with significantly lower amplitude (more than 2 decades less for probe 3 and
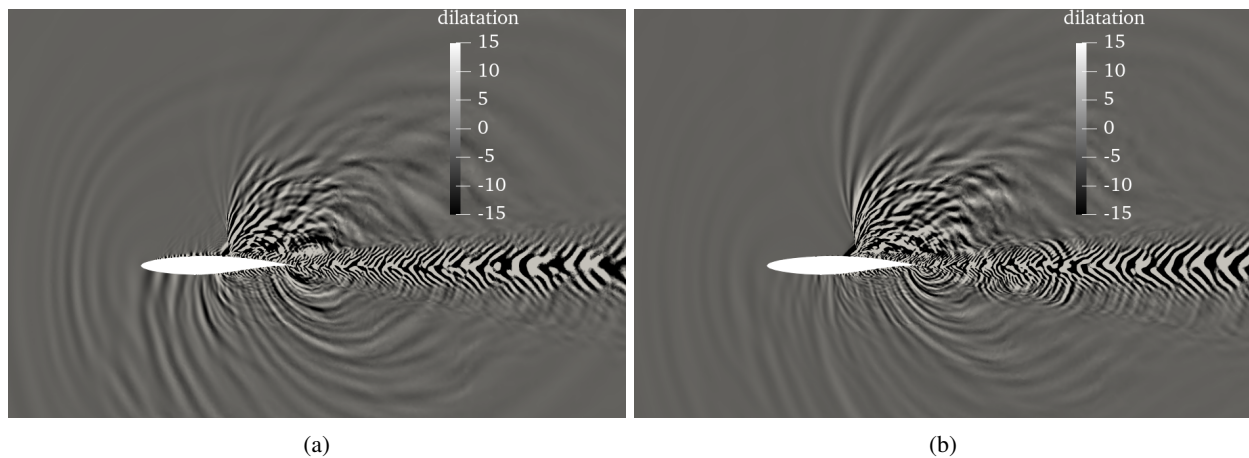
Figure. 8: Dilatation field for - (a): LES 1 and (b): LES 2.

one decade less for probe 4). This observation confirms what the previous observations for the Q-criterion, that is, the LES 2 supersonic laminar boundary layer region (before the shock-wave) has a significantly less strong instability. However, the presence of the peaks at 10 kHz indicates again that some high-frequency instability may still be present (as seen in the time trace of probe 4, Fig. 5). On the pressure side, the behavior of both simulations is similar for probes 7 and 11, located after the transition to turbulence. On the other hand, the peaks present in probe 5 of LES 1 (at 20–30 kHz and 50 kHz) disappear in LES 2. Such peaks were attributed by [8] to the presence of a laminar separation bubble (LSB). The disappearance of the peak in LES 2 can be caused by either the disappearance of the LSB, or by the displacement of its location. This will be confirmed in a future work, by adding additional probes on the pressure side.

IV. ACOUSTIC RESULTS

As in Koch *et al.* [8], the acoustic results are analyzed in two steps. A visualization of the dilatation field is first shown in Fig. 8, comparing LES 1 and LES 2. The radiation pattern for both simulations is similar. Nonetheless, a difference is seen on the suction side, inside the supersonic pocket. LES 1 shows a pattern appearing at such a location. On the same scale this pattern disappears in LES 2. Thus, it is seen that the noise source associated with the instability wave reduces its amplitude or even completely disappears when employing the new mesh. This highlights the interest of the present work, since the mesh effects (*e.g.* a too sharp transition in the surface mesh) can create nonphysical acoustic sources.

In order to provide more quantitative acoustic results, far-field noise pressure spectra are obtained from both LES results with a Ffowcs Williams and Hawkings (FW-H) analogy. This analogy propagates the noise pressure fluctuations from the airfoil surface to the far field. The software used for the FW-H computation is the in–house code called SherFWH and is based on the advanced time approach for acoustic analogy predictions from Casalino [14]. It uses a solid surface, corresponding to the airfoil surface. For LES 1, the unsteady wall-pressure signal is recorded with a sampling frequency

of 125 kHz, and with a cut-off frequency of 50 kHz at the solid surface. For LES 2, the sampling and cut-off frequencies are 250 kHz and 50 kHz, respectively, since the LW scheme requires 16 points per wavelength (around 0.4 mm in cell size). The resulting pressure levels calculated with the FW-H analogy are calculated at observers located on a circle at 2 m from the trailing edge at midspan for different angular positions, as depicted in Fig. 7. The PSD of such pressure probes for LES 1 and LES 2 are compared (black and red lines) in Fig. 9. The PSD is obtained with the Welch's periodogram method [13], using time windows of length $T/3$ with 50% overlap as used to compute the PSD. It yields a total of 5 blocks, windowed with a Hanning function. For LES 1, an acoustic signal of $T = 51$ ms is employed, while for LES 2, $T = 20$ ms is used. Thus, the frequency resolution of the PSD spectra is equal to $\Delta f = 50$ Hz for LES 1 and $\Delta f = 150$ Hz for LES 2. The low frequency part of the spectra under $10\Delta f$ is under-resolved and can present nonphysical oscillations. This gives a minimum frequency of 500 Hz for safe physical interpretations in LES 1 and 1500 Hz in LES 2.

The results show that the spectra between LES 1 and LES 2 are similar, except at $\theta = 45°$, where LES 2 levels are around 5 to 10 dB higher than the ones of LES 1 between 10 to 20 kHz. This increase in the radiation downstream of the shock may be an effect of the highly directive emission of the shock. Future work should study the directivity of the sound emission by increasing the number of observers in the 2 m arc around the airfoil. Finally, the high-frequency pressure hump between 30 and 40 kHz is still present in LES 2. This suggests that such a high-frequency noise directed towards the upstream direction is not linked to the flow instability encountered in the supersonic pocket, on the suction side of LES 1. In order to identify this source, a filtering of the dilatation fields around this frequency such be performed.

V. CONCLUSION

In this work, a LES on the RAE 2822 airfoil is performed, operating in the transonic regime. Extending the previous work by Koch *et al.* [8], a new mesh has been generated, in order to study the possible origin of a potential noise source created
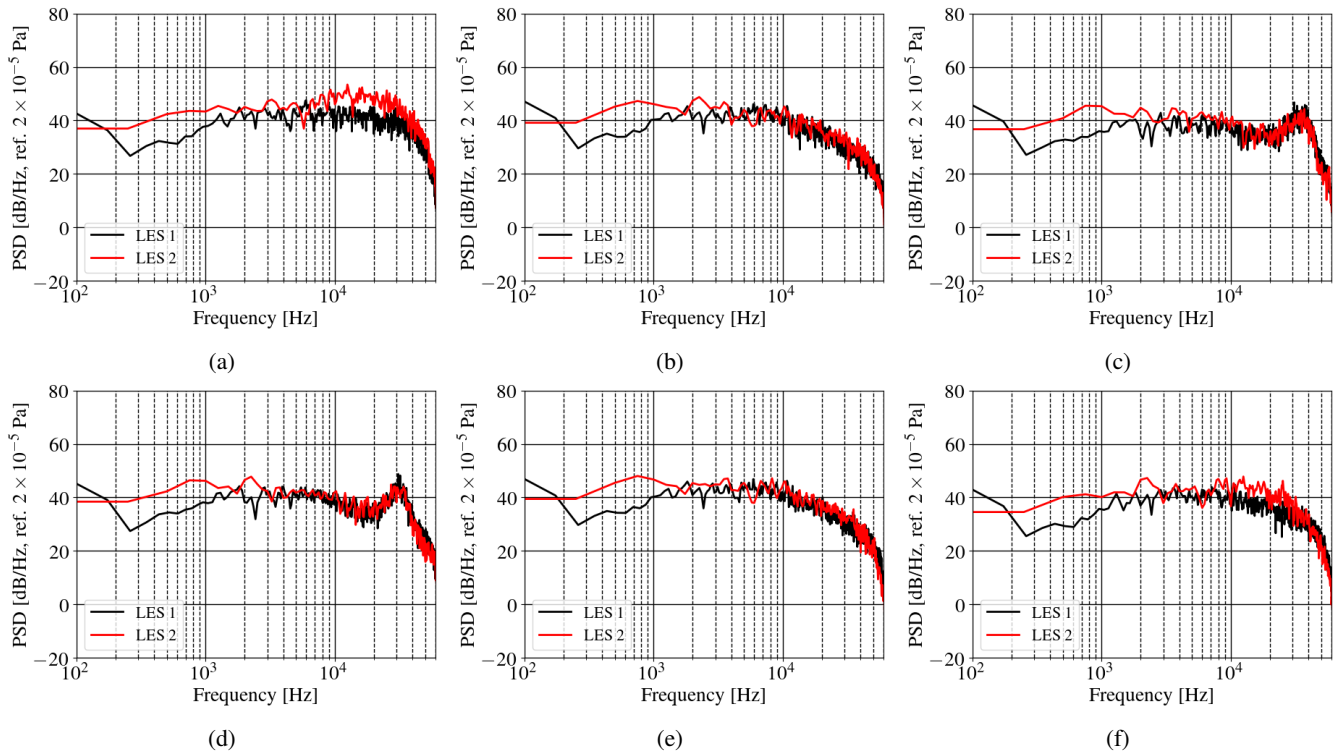
Figure. 9: PSD of far-field mics using the FW-H analogy solid formulation, for (black lines) LES 1 and (red lines) LES 2, for different observers located on a circle centered at 2 m from the trailing edge, at midspan - (a): $\theta = 45°$; (b): $\theta = 90°$; (c): $\theta = 135°$; (d): $\theta = 225°$; (e): $\theta = 270°$; (f): $\theta = 315°$.

by a jump in the suction side surface mesh. The aerodynamic results show that the hydrodynamic instabilities present in the baseline configuration are significantly decreased on the new mesh. This is confirmed by the analysis of the unsteady wall-pressure probes spectra. A FW-H analogy, using the solid surface formulation, is employed to study the acoustic emissions of the airfoil. Both simulations (baseline and new mesh) show very similar results, indicating that the flow instabilities were not responsible for the high-frequency noise source observed at 30–40 kHz. The source of this peak remains unclear and will be investigated in future works.

REFERENCES

[1] R. Koch, M. Sanjose, S. Moreau, Large-eddy simulation and broadband acoustic prediction of an helicopter rotor in hover, in: 28th AIAA/CEAS Aeroacoustics Conference, Southampton, UK, june 2022, pp. AIAA 2022–2915. doi:10.2514/6.2022-2915.

[2] P. Kholodov, M. Sanjosé, S. Moreau, Fan Broadband Noise Computation at Transonic Regime, in: 25th AIAA/CEAS Aeroacoustics Conference, AIAA 2019-2655 paper, Delft, Netherland, 2019.

[3] P. Cook, M. Firmin, M. McDonald, Aerofoil rae 2822: pressure distributions, and boundary layer and wake measurements, AGARD Report AR 138 (1977).

[4] P. Catalano, M. Amato, An evaluation of rans turbulence modelling for aerodynamic applications, Aerospace science and Technology 7 (7) (2003) 493–509.

[5] T. Yu, J. Wang, P. Zhang, Numerical simulation of gurney flap on rae-2822 supercritical airfoil, Journal of Aircraft 48 (5) (2011) 1565–1575.

[6] Z. Xiao, H. Chen, Y. Zhang, J. Huang, S. Fu, Study of delayed-detached eddy simulation with weakly nonlinear turbulence model, Journal of aircraft 43 (5) (2006) 1377–1385.

[7] N. Tonicello, High-order spectral element methods for the simulation of compressible turbulent flows, Ph.D. thesis, University of Rouen (2021).

[8] R. Koch, M. Sanjosé, S. Moreau, Acoustic investigation of the transonic rae 2822 airfoil with large-eddy simulation, in: 28th AIAA/CEAS Aeroacoustics Conference, Southampton, UK, june 2014, pp. AIAA 2022–2816. doi:10.2514/6.2022-2816.

[9] T. Schönfeld, M. Rudgyard, Steady and Unsteady Flow Simulations Using the Hybrid Flow Solver AVBP, AIAA Journal 37 (11) (1999) 1378–1385.

[10] T. J. Poinsot, S. Lelef, Boundary conditions for direct simulations of compressible viscous flows, Journal of computational physics 101 (1) (1992) 104–129.

[11] N. Odier, M. Sanjosé, L. Gicquel, T. Poinsot, S. Moreau, F. Duchaine, A characteristic inlet boundary condition for compressible, turbulent, multispecies turbomachinery flows, Computers & Fluids 178 (2019) 41–55.

[12] F. Nicoud, F. Ducros, Subgrid-scale stress modelling based on the square of the velocity gradient tensor, Flow, turbulence and Combustion 62 (3) (1999) 183–200.

[13] P. Welch, The use of fast fourier transform for the estimation of power spectra: a method based on time averaging over short, modified periodograms, IEEE Transactions on audio and electroacoustics 15 (2) (1967) 70–73.

[14] D. Casalino, An advanced time approach for acoustic analogy predictions, Journal of Sound and Vibration 261 (4) (2003) 583–612.